Applied Catalysis B: Environmental 88 (2009) 272–282

Contents lists available at ScienceDirect

Applied Catalysis B: Environmental

journal homepage: www.elsevier.com/locate/apcatb

A comparative study of water gas shift reaction over gold and platinum supported on ZrO_2 and CeO_2–ZrO_2

Marta Boaro [a], Michela Vicario [a], Jordi Llorca [b], Carla de Leitenburg [a], Giuliano Dolcetti [a], Alessandro Trovarelli [a,*]

[a] Dipartimento di Scienze e Tecnologie Chimiche, via del Cotonificio 108, Università di Udine, 33100 Udine, Italy
[b] Institut de Tècniques Energètiques, Universitat Politècnica de Catalunya, Diagonal 647, ed. ETSEIB, 08028 Barcelona, Spain

ARTICLE INFO

Article history:
Received 9 September 2008
Received in revised form 3 November 2008
Accepted 9 November 2008
Available online 17 November 2008

Keywords:
Gold
Platinum
Zirconia
Ceria–zirconia
WGSR
Hydrogen

ABSTRACT

In this study platinum- and gold-based catalysts supported on ZrO_2 and ceria–zirconia solid solution have been characterized by several techniques (TPR, XRD, BET, HRTEM) and tested in the water gas shift (WGS) reaction under feed conditions typical of an autothermal reformer outlet. Platinum and gold catalysts behave differently especially in the range of 423–513 K, with gold being superior than platinum. The possibility of modifying the redox and structural characteristics of zirconia with the insertion of ceria allowed us to conclude that the bulk redox properties of the support play a secondary role, while the key parameter for an active WGS catalyst is the nature of metal support interface. This, in turn, depends on the metal particle distribution and on the structural and morphological properties of support. It has been found that the synergism between precious metals and support can be designed with an appropriate choice of the parameters of synthesis and the characteristics of support.

1. Introduction

The water gas shift (WGS) reaction is an important step in a number of chemical processes for the production of H_2. Although the WGS technology is well established and widely used in large scale steady-state operations, such as hydrogen or ammonia plants, the interest has been growing significantly in the last few years, as a result of the advancements in fuel cell technology [1,2]. In particular, industrial low temperature WGS catalysts are not applicable for most fuel processing applications without significant engineering and control strategies [3]. Because of the slow kinetics observed at low temperature the WGS unit is expected to be the largest component of a fuel processor [4] and the strong necessity to reduce the volume and the weight of the whole processor has driven the research to develop more active WGS catalysts with properties fundamentally different from those of industrial use [5]. In fact, an ideal WGS catalyst should not require in situ activation and not be pyrophoric, moreover it should have high tolerance to temperature excursion and to exposure to condensing and oxidizing conditions during the many expected start up and shut down cycles.

Recently, a few studies have reported about commercial compositions with satisfying properties [6,7]. The most active formulations are based on noble and transition metals supported on reducible oxides [8–12]; however, an increase of the activity by order of magnitude is necessary in order to obtain materials economically viable and competitive with the traditional ones.

Platinum [13–18]- and gold [19–25]-based catalysts are largely investigated with gold offering the advantage to be substantially cheaper and more plentiful [26,27]. As far as we know only a few studies compare platinum and gold catalysts under real WGS conditions addressing the issue of support reducibility [28–32]. Since gold nanoparticles adsorbs CO more weekly than platinum [33] it is expected that the reaction mechanism for gold-based catalysts will be different from that of platinum-based systems. However, it would be difficult to draw general conclusions from the data available in the literature because the activity of WGS catalysts depends strongly on the methods of preparation [34,35], the characteristics of support [36] and the conditions of testing. In particular, in the case of reducible oxides as supports, the atmosphere of reaction and pretreatment conditions control the degree of reducibility and this, in turn, determines the nature of interaction with the metal and the overall reactivity of the system.

In this work the shift activity of gold-based catalysts on zirconia and on ceria–zirconia solid solution is compared with that of platinum catalysts in order to clarify the characteristics of each

* Corresponding author.
E-mail address: trovarelli@dstc.uniud.it (A. Trovarelli).

0926-3373/$ – see front matter © 2008 Elsevier B.V. All rights reserved.
doi:10.1016/j.apcatb.2008.11.010

system and to understand the key parameters for developing and optimizing an effective catalyst for WGS.

The choice of zirconia as support is due to the chemical and physical property of the oxide. Zirconia has several polymorphs, which exhibit different surface catalytic sites, such as hydroxyl groups and coordinative unsaturated Lewis acidic-base Zr^{4+}–O^{2-} pairs, which can influence the behavior of CO adsorption and reaction [37,38]. Recently, platinum supported on monoclinic and tetragonal zirconia has been investigated in order to elucidate the role of bridge hydroxyl groups into the formation of water gas shift intermediates [16]. In addition, nanostructured zirconia exposed to specific reduction conditions shows the formation of F-centres, i.e. electrons trapped in oxygen vacancies, which affect the charging of support surface and consequently the nature of metal-support interaction. This may be also among the reasons of the dramatic increase of activity of Au/oxides catalysts in CO oxidation [39]. Zirconia and ceria–zirconia mixed oxides have also been shown as suitable and active supports for gold-based water gas shift catalysts [24,40–42]; the benefit might result from the formation of a solid solution between ceria and zirconia that stabilizes the cubic or the tetragonal structure of the oxide, with additional significant effects on the reducibility of materials and on the oxygen uptake/release features from both the surface and bulk of the oxide [43]. Among the compositions available, solid solutions with intermediate Ce/Zr loading shows optimal redox properties with stabilization of the cubic/tetragonal phase [44].

In this work the behavior of cubic $Ce_{0.44}Zr_{0.56}O_2$ has been compared to that of pure zirconia supported catalysts in order to elucidate the role of structure and redox properties of the support into the water gas shift mechanism. High-resolution transmission electron microscopy (HRTEM) analysis and temperature programmed reduction (TPR) measurements have been carried out in order to distinguish the properties that mostly affect the activity of these compositions and that can be engineered by an appropriate methodology of synthesis.

2. Experimental

2.1. Materials

The supports used $Ce_{0.44}Zr_{0.56}O_2$ and ZrO_2 (that will be indicated through the text as CZ44 and CZ0) were supplied respectively by Grace Davison (USA) and MEL Chemicals (UK). They have been calcined at temperatures in the range 723–1123 K in order to obtain a series of homogeneous samples with high surface area (HSA samples, 70–80 m^2/g) and low surface area (LSA samples, 35–40 m^2/g).

Gold catalysts (loading 4 wt.%) were prepared by deposition precipitation using $HAuCl_4{\cdot}3H_2O$ (Aldrich) as precursor. The support material was thoroughly suspended in deionized water and the pH adjusted around 8 by adding $(NH_4)_2CO_3$ [45]. A 10^{-3} M aqueous solution of gold precursor was added slowly drop by drop to the slurry [20]. The resulting precipitate was aged at room temperature for 1 h under agitation and then filtered and washed with deionized water until the $AgNO_3$ chloride test turned into negative. All the samples were dried at 383 K overnight and then calcined at 523 K or higher temperature for 1 h. Platinum was deposited by incipient wetness impregnation with a nominal loading of 4 wt.%. The support was first dried and then impregnated with an aqueous solution of $Pt(NH_3)_4(NO_3)_2$–Pt(N) samples or $H_2PtCl_6{\cdot}6H_2O$–Pt(Cl) samples from Aldrich. The solution was added dropwise, incorporating the catalyst precursor until saturation of pores. To achieve the desired loading, the impregnation was repeated three or four times. The samples were dried at 383 K overnight, crushed and calcined at 823 K for 1 h under air flow.

2.2. Characterizations of materials

Nitrogen adsorption–desorption isotherms for BET surface area and BJH pore size and pore size distribution measurements were made with a Micrometrics TRISTAR 3000 gas analyzer at 77 K over a wide relative pressure range from 0.03 to 0.995.

X-ray powder diffraction profiles were collected with a Philips PW3040/60 X'pert PRO instrument (equipped with an X'celerator detector) operated at 40 kV and 40 mA, with Ni-filtered Cu-K_α radiation. Diffraction profiles were collected in the 2θ range of 20–145° with a step width of 0.02° and a counting time of 40 s/step. The average size of oxide particles was determined from XRD line broadening by Scherrer's equation.

Microstructural characterization by high-resolution transmission electron microscopy was carried out with a JEOL 2010F instrument equipped with a field emission gun, which allowed to achieve a point-to-point resolution of 0.19 nm and a resolution of 0.14 nm between lines. Samples were deposited directly on holey-carbon coated grids.

CO-temperature-programmed reduction (CO-TPR) studies were conducted in a customized apparatus [46], which was equipped with a mass spectrometer analyzer (Balzer Q-Star) and a micro-gas chromatograph (Varian). About 0.150 g of sample were flushed with a He flow for 1 h at room temperature, then a stream of 5% CO in He was fed at 35 ml/min as the catalyst temperature was increased from 298 to 1273 K at a ramp rate of 10 K min^{-1}. This approach is very suitable to study the fresh catalysts without introducing any metal-support interface alteration or changes in the reduction state of the ceria-based support. The suitability of the pretreatment to remove carbon dioxide and water from the surface of the catalysts was checked on some samples carrying out TPRs with and without a thermal treatment at 423 K, very similar profiles have been obtained. The quantitative analysis of reactants and products was carried out by the integration of the TPR profiles obtained from the measured CO, CO_2 and H_2 concentrations of sequential chromatograms.

2.3. Catalytic tests

Steady-state shift activity was tested by loading about 0.170 g of catalyst in a quartz tube (16 in. length, 0.25 in. Ø). The operating conditions were chosen to mimic those existing in a LT-WGS reactor for fuel processing with an inlet feed composition of 39% H_2, 24% N_2, 6% CO, 10% CO_2, and 21% H_2O with a space velocity of 40,000 h^{-1}. The water was delivered with a precision syringe and the line before the reactor was kept at 473 K by heating tapes. Before testing the catalysts were activated at 453 K under a 5% H_2 in helium flow (50 ml/min). The temperature was increased from 453 to 623 K in six/seven steps. For every temperature the reactants and products were monitored by a two columns HP5990 gas-chromatograph with a TCD and a FID detector. The measured conversion was calculated by averaging the results of the three last chromatograms after equilibration at a steady state. The water was condensed before the GC analyzer with a refrigerator and quantified indirectly from the changes in the total flow rate using nitrogen as internal standard. The equilibrium conversion was calculated using the package software HSC (Outokumpu).

3. Results and discussion

3.1. Morphological and structural characterization

Two series of support samples were prepared with surface area respectively in the range of 80–70 m^2/g (HSA) and 35–40 m^2/g (LSA). This was done before metal deposition by calcining the oxides at different temperatures, chosen according to the thermal

Table 1
Morphological and structural characteristics of HSA and LSA samples.

Sample	Support composition	Calcination temperature (K)		Surface area[a] (m^2/g)		Crystalline structure[b]		Cumulative pore volume[c] (cm^3/g)		Crystalline size[d] (nm)	
		HSA	LSA	HSA	LSA	HSA	LSA	HSA	LSA	HSA	LSA
CZ44	$Ce_{0.44}Zr_{0.56}O_2$	923	1123	68	34	c	c	0.193	0.152	5	8
CZ0	ZrO_2	723	923	81	38	m/t	m/t	0.119	0.085	9	14

[a] BET measurements.
[b] c = cubic, m = monoclinic and t = tetragonal—determined by XRD.
[c] BJH desorption measurements.
[d] Calculated from XRD by Scherrer's equation.

Table 2
Morphological and structural characteristics of catalysts.

Samples[a]	Calcination temperature (K)	Noble metal phase[a]	Mean metal particle size[a] (nm)	BET surface area (m^2/g)
Au/CZ44-LSA	523	Au	2.0	33
Au/CZ0-LSA	523	Au	2.7	35
Au/CZ44-HSA	523	Au	1.7	67
Au/CZ0-HSA	523	Au	nd	73
Au/CZ44-LSA	723	Au	5.2	33
Au/CZ0-LSA	723	Au	5.4	35
Pt(N)/CZ44-LSA	823	PtO	2.3	30
Pt(N)/CZ0-LSA	823	nd	1.5[b]	37
Pt(Cl)/CZ44-LSA	823	PtO_2	4 (3.4)[c]	29
Pt(Cl)/CZ0-LSA	823	PtO_2	5 (3.2)[c]	37
Pt(Cl)/CZ44-HSA	823	PtO_2	1 (2.3)[b]	61
Pt(Cl)/CZ44-HSA	623	PtO_2	nd[d]	61

[a] From HRTEM measurements.
[b] Determined from the dispersion measured by H_2 chemisorption at 183 K with a Micromeritics ASAP 2020 analyser assuming a chemisorption stoichiometry H:Pt = 1:1.
[c] After reduction at 423 K.
[d] Particles not detectable from HRTEM.

resistance of the different compositions. The morphological and structural characteristics of the resulting supports and of the catalysts obtained after deposition are summarized respectively in Tables 1 and 2. Zirconia is mainly monoclinic with a small fraction of tetragonal phase; the incorporation of ceria instead stabilizes the cubic phase. The deposition of gold and platinum resulted in a slight reduction of surface area and porosity of the supports while the pore size distribution curves were centered at around 40 and 90 Å respectively for zirconia and ceria–zirconia solid solution (results not shown).

Fig. 1 shows the HRTEM micrographs of gold supported on ceria–zirconia and on zirconia substrates. A and B images refer respectively to Au/CZ44-LSA and Au/CZ0-LSA catalysts calcined at 523 K, while 1C and 1D to the corresponding catalysts calcined at 723 K. On ceria–zirconia (1A) gold particles are labeled as "a"–"f" and enlarged with their lattice spacings in the right side. In these details the lattice spacing at 2.35–2.36 Å corresponds to Au (1 1 1) planes. On zirconia support (1B) the presence of Au is revealed by Fourier transform analysis in the center of area B. In both case no evidence for Au oxides was encountered. Therefore, from lattice-fringe analysis it is possible to conclude that when gold precursors have been calcined at low temperature (523 K) gold particles were distributed homogeneously on both ceria–zirconia and zirconia supports in very small mostly round-shaped monocrystallites. The exact distribution of particle size (obtained by analyzing ca. 150 particles) are included in Fig. 2. The size distribution of gold particles was centered at 2.2 nm in a very narrow interval on CZ44-LSA (2A, empty bar) and in a slightly broader distribution, centred at 2.7 nm, on CZ0-LSA (2B, empty bar).

The increase of calcination temperature of gold precursors caused a growth of crystallite size and a broader distribution of sizes. The respective particle size distributions are now centered at 5.2 nm in the case of ceria–zirconia (2A, black bars) and at 5.6 nm in zirconia (2B, black bars). Moreover Fig. 1C and D, corresponding respectively to 1A and 1B samples calcined at 723 K, showed that most of gold particles changed their rounded shape to a well-developed crystallographic faceted form. Even in this case the lattice-fringe analysis indicated that only metallic Au composed the particles. These results suggest that, at least under our experimental conditions, the final gold particle size distribution reflects the initial distribution of precursors that, in turns, is affected by the adopted parameters of synthesis more than on the nature and structure of supports.

Fig. 3 shows HRTEM results related to platinum-based catalysts. The images 3A and 3B refer to platinum deposited respectively on CZ44-LSA and on CZ0-LSA. In Fig. 3A the Fourier transform images of "a" and "b" are also included. Spots at 3.05 and 2.66 Å in "b" correspond to the (1 1 1) and (2 0 0) planes of cubic CZ44, respectively, whereas spots at 3.20 Å in "a" correspond to PtO_2 (1 1 0) planes. From these images it has been established that the deposition of platinum from chloride precursors occurs through the formation of small crystallites of PtO_2 without any apparent structural relationship with the support. Their shape is rounded not faceted and their size was calculated from several micrographs to be about 4 nm in ceria–zirconia and about 5 nm in zirconia supported catalysts. More detailed information on platinum particle size distributions have been shown in Fig. 4A and B in which the empty bars refer to PtO_2 particles distributions, while the black bars are related to the distributions of platinum particles after hydrogen reduction of samples at 423 K. Concerning the reduced samples, it is clear that the mean particle size slightly decreases in both Pt/CZ0-LSA and Pt/CZ44-LSA, which could be interpreted in terms of particle disruption during reduction. It turns out that the final particle size and distribution in both samples is similar (3.2 nm vs. 3.4 nm).

Further HRTEM analysis on platinum-based catalysts has pointed out the importance of other parameters in controlling the platinum crystallite size distributions. Fig. 3C shows an image

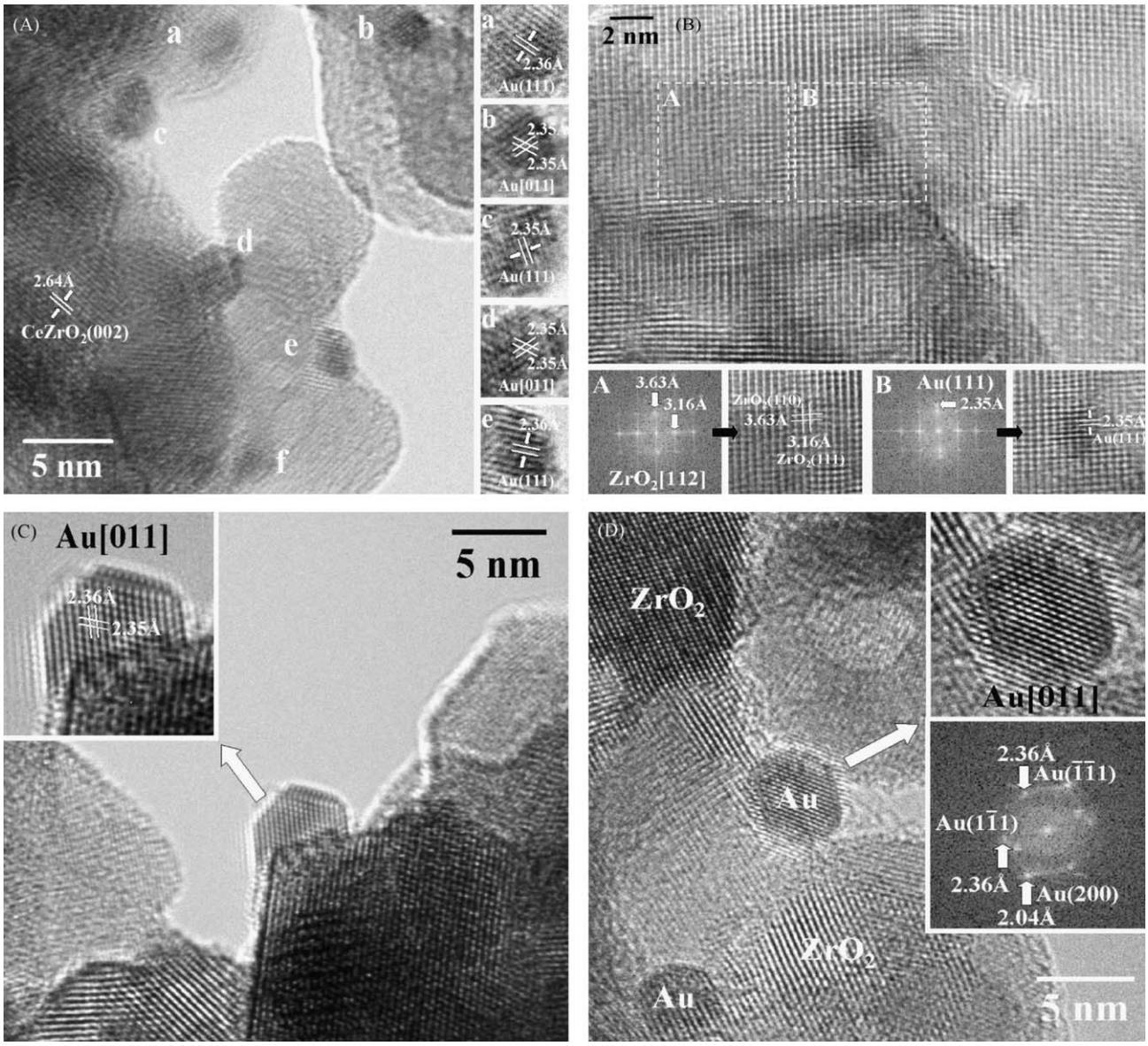

Fig. 1. HRTEM images of (A) Au/CZ44-LSA calcined at 523 K, (B) Au/CZ0-LSA calcined at 523 K, (C) Au/CZ44-LSA calcined at 723 K and (D) Au/CZ0-LSA calcined at 723 K.

of the ex-chloride platinum catalyst supported on high surface area ceria–zirconia solid solution as representative example to investigate the effect of the surface area. In this micrograph, platinum-containing particles are extremely tiny with a distribution size in the range 0.5–1.5 nm. In this case, due to their small size it was not possible to obtain lattice-fringe images of individual Pt-containing particles (marked by arrows). The comparison with the image 3A shows that the difference in particle size between HSA and LSA CZ44 supported catalysts is large (1 nm vs. 4 nm) and the size distribution of Pt-crystallites has been strongly affected by the surface area of the support. Furthermore, Fig. 3D, which shows the HRTEM image of the ex-nitrate platinum catalyst Pt(N)/CZ44-LSA, reveals that another parameter able to influence the size and distribution of metal is the nature of precursors. In this later micrograph the area labeled "a" corresponds to a single CZ crystal oriented along the [1 1 1] crystallographic direction while the area labeled "b" corresponds to a PtO crystallite supported on CZ. In this case the thermal decomposition of $Pt(NH_3)_4(NO_3)_2$ leads to very small PtO crystallites with a size distribution in the range of 1.6–3 nm, that after reduction became platinum crystallites with a mean particle size of 1.5 nm (results not shown). The same result has been found by hydrogen chemisorption technique (see Table 2) for Pt(N)/CZ0-LSA.

To summarize, HRTEM results of platinum samples showed that the composition of support does not play a significant role in controlling the final size and the distribution of platinum crystallites. Significant parameters affecting the particle size distribution are the surface area, with higher values stabilizing narrower distributions, and the Pt precursors, with nitrates giving smaller platinum crystallites than chlorides, leading to higher dispersion values.

3.2. Catalytic activity

The morphological characteristics and the metal particle size distributions are strongly correlated with the catalytic activity of these catalysts. Fig. 5 shows the effect of the temperature of calcination of the metal precursors on the catalytic activity of samples. The study has been carried out on low surface area supported catalysts in order to deal with supports already

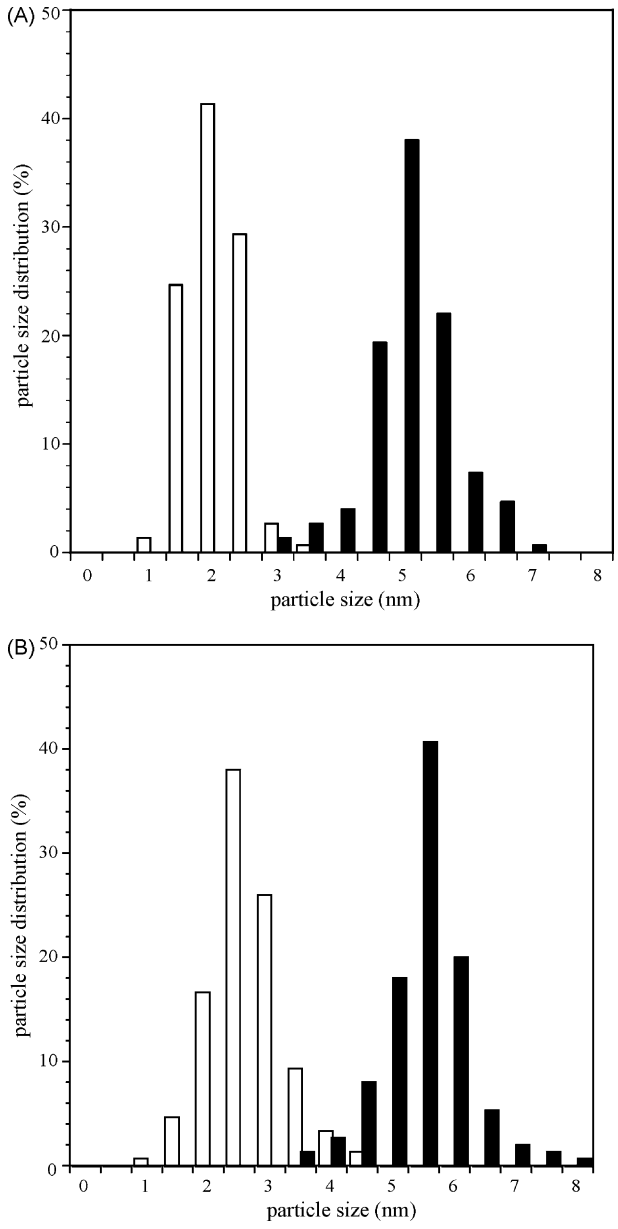

Fig. 2. Particle size distribution calculated from HRTEM measurements of (A) Au in Au/CZ44-LSA calcined at 523 K (empty bar) and at 723 K (filled bar), and (B) Au in Au/CZ0-LSA calcined at 523 K (empty bar) and at 723 K (filled bar).

stabilized to the chosen temperature of calcination. The thermal treatment after the metal deposition affected remarkably the activity of both platinum and gold catalysts, but in opposite way. In the case of platinum (Fig. 5A) a gradual improvement of the performance was observed as the calcination temperature was increased to 823 K. TGA measurements and elemental analysis of chlorides suggested that the improvement of catalytic activity with the calcination of temperature is due to an incomplete decomposition of chloride precursors (reached only at temperature higher than 823 K). This is in agreement with the fact that, under oxidizing atmosphere, $H_2PtCl_6{\cdot}6H_2O$ decomposes releasing chlorine at temperature as high as 793 K [47]. In our samples the percentage of chlorides has been found to decrease from 1 to 0.5 wt.% as the temperature of calcination increases from 623 to 823 K.

In contrast, for gold catalysts, an increase of the calcination temperature caused a decrease of activity (Fig. 5B). HRTEM analysis revealed that the deactivation of gold catalysts is correlated with a sintering process of gold particles that causes an increase of the size and consequently a change of shape from hemispherical round to well-faceted crystallites. These phenomena induce respectively a decrease of the perimeter zone and a modification of the nature of active centers. In fact, a change on geometries could lead to a variation of the distribution and nature of defects on gold nanoparticles. This latter aspect may be of importance because previous reports in literature claim such defects as possible sites on which CO oxidation could take place [48–50]. It is worth mentioning that the effect of calcination temperature depends on the nature of support, with the highest deactivation observed for gold catalyst supported on ceria–zirconia. At present, we have not an exhaustive explanation for this result. However, since size and shape of gold particles underwent modifications of the same entity independently on the composition of support (see HRTEM analysis), we suppose that the reasons for the different behavior could be found in the characteristics of the supports and their interaction with the metal. From DFT calculations it has been suggested that under water gas shift conditions in Au/CeO_2 and $Au/CeZrO_4$ catalysts the active sites are small metal clusters in full contact with the support surrounded by oxygen vacancies [51,52] and that deactivation occurs as the gold particle gradually looses contact with the supports. Deactivation of Au/CeZrO4 catalysts during low-temperature WGS test has also been observed as water concentration was raised [53]. The authors suggested that the mechanism of dewetting was due to hydrolysis at the interface between gold particles and the support promoted by the oxygen vacancies close to the metal cluster. Similar mechanism was proposed to explain the thermal deactivation observed for catalysts of analogues composition; heating causes a detachment of the $Au^{\delta+}$ adatoms stabilized on cationic lattice vacancies with loss of the anchoring points for the nanoparticles [42,52]. It is likely that in this mechanism the kinetics of the process can be favored by the high mobility of surface oxygen ions of the ceria–zirconia support, oxygen ions migrate to the gold particle-oxide interface filling the oxygen vacancies. This would contribute to the weakening of the bonding between gold cluster and support in a manner similar to what occurs for the water-induced deactivation. Several studies underline the importance of the presence of vacancies and defects close to the metal particle interface in order to stabilize and activate them [42,49,54]. A strong interaction between gold and support is also the key factor for the high activity of Au/ZrO_2 catalysts on the CO oxidation and water gas shift reaction [38,55]. We believe that a loss of contact between gold and support is also the cause of the minor activity of the Au/CZ0 high temperature calcined catalyst. Therefore, the differences of the degree of deactivation observed for the two supports in relation to the temperature of calcination could be attributed to a different kinetics of formation and deactivation of the active sites, due in part to the high difference of mobility of surface oxygen ions on the two supports. IE studies demonstrate that at 623 K the surface diffusion coefficient of oxygen ions for ceria is two order of magnitude higher than for zirconia [56]. To conclude from our results is clear that that the particle–support perimeter is the scene of cooperative effects where both the support and the metal participate to the catalytic process; moreover it is possible to deduce that the nature of the support itself is very important for determining the activity of these systems.

Figs. 6 and 7 show the effect of surface area and support composition on the catalytic activity respectively for platinum and gold-based catalysts. By comparing gold and platinum catalysts, it is worthy to note that they behave differently especially at low temperature. For platinum-based catalysts the conversion remains lower than 20% until 500–523 K and then it increases sharply to the equilibrium value at 563–573 K. Actually, in this range of temperature the final conversion overcomes slightly the equilibrium value due to a small methanation activity. For all the catalyst tested, methanation occurs from 573 K and increases with

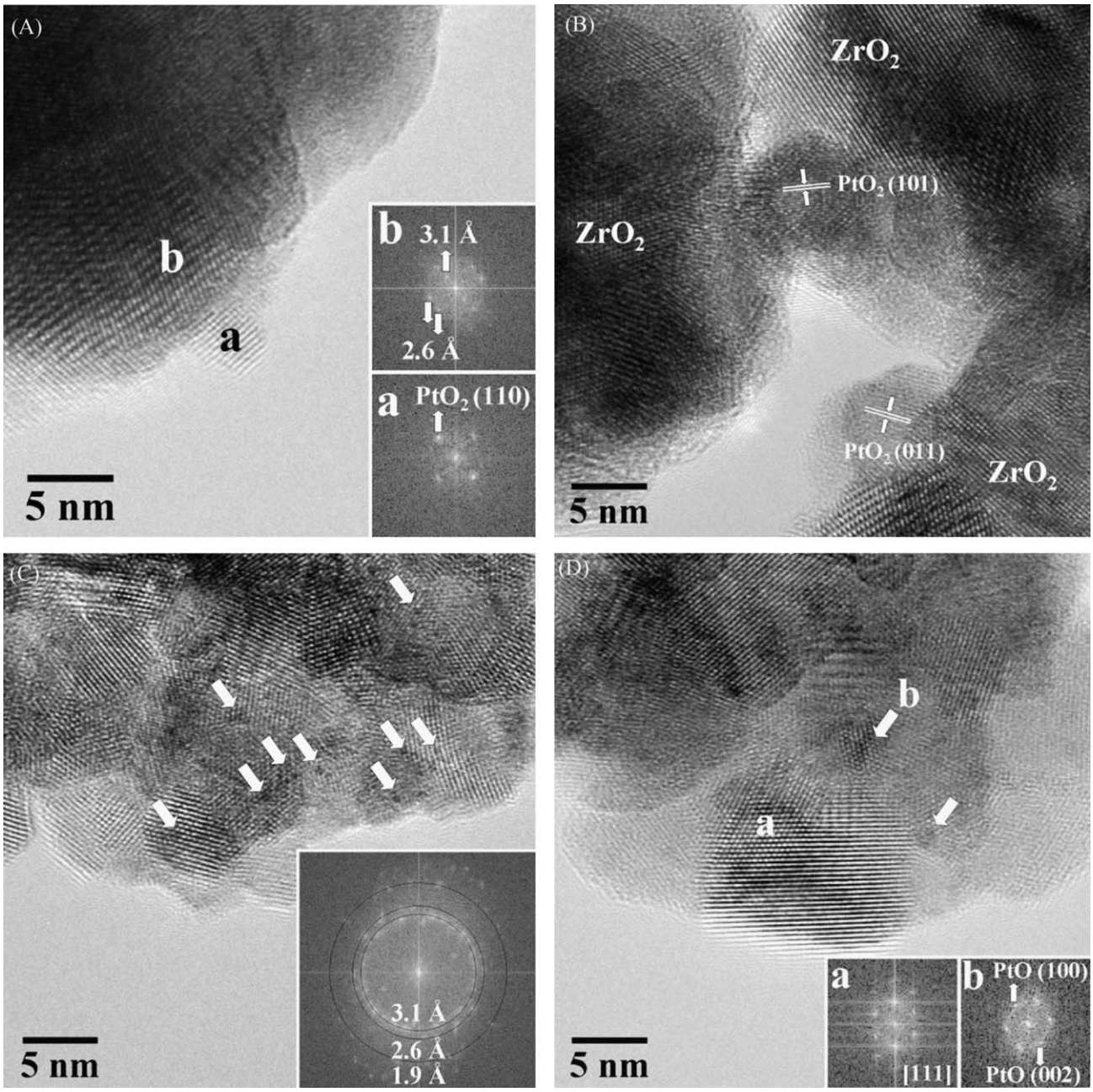

Fig. 3. HRTEM images of Pt-based catalysts. (A) Pt(Cl)/CZ44-LSA calcined at 823 K; (B) Pt(Cl)/CZ0-LSA calcined at 823 K; (C) Pt(Cl)/CZ44-HSA calcined at 823 K; (D) Pt(N)/CZ44-LSA calcined at 823 K.

temperature reaching conversion of ca. 5%. In contrast, Au catalysts show an appreciable conversion (20–50%) already at 453–473 K, and then the conversion increases smoothly approaching equilibrium values at almost 603 K, while methane production is not observed. This behavior has been already reported in literature [42,57,58] and it is in part related to the weaker adsorption of CO on gold than on platinum crystallites [59]. The energy of adsorption of CO on Au_2—CO cluster has been recently estimated by DFT to be 27 kcal/mol versus the 45 kcal/mol for the corresponding Pt_2—CO [33]. For platinum and gold catalysts the water gas shift occurs through a dual site mechanism where the support provides active sites for the splitting of water and the metal particles provide sites for the adsorption of CO. The two main mechanisms proposed in the literature are a ''regenerative'' and an ''associative'' mechanism and recently it is suggested that the same catalyst can follow both the mechanisms depending on the testing conditions [42]. At temperature of 453–473 K it is more likely to be operative an associative mechanism where the formation of active formate intermediates requires the participation of CO from the metal and the OH groups from the support. In this kinetics a faster diffusion of CO adsorbates, due to a weaker bond with the metal particles, could favor the shift reaction at lower temperature.

Another significant difference between Au and Pt systems is related to the effect of morphology of support. The activity of gold catalysts is almost independent on the surface area of supports whereas the activity of platinum catalysts improves, especially in the range of light-off temperatures, when platinum has been dispersed on oxides with a high surface area. This is because the dispersion of platinum increases with the surface area of supports as already shown in Fig. 3C and D for ex-chloride Pt catalysts supported on CZ44-LSA and on CZ44-HSA. The results reported in

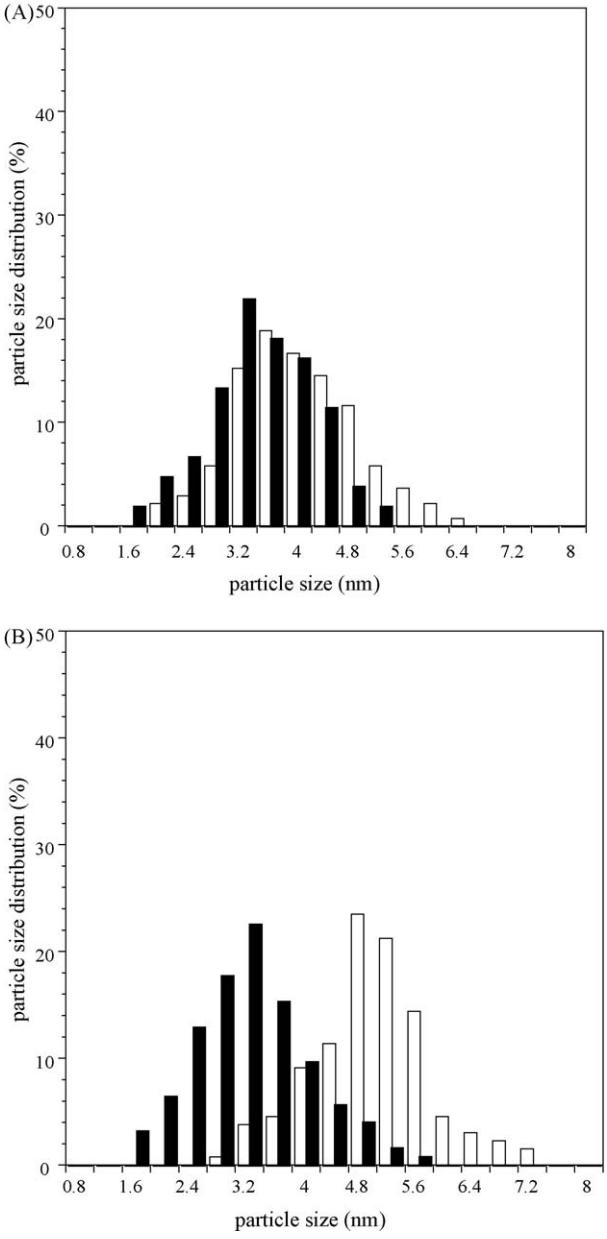

Fig. 4. Particle size distribution calculated from HRTEM measurements of (A) PtO_2 in Pt/CZ44-LSA calcined at 823 K (empty bar) and Pt in Pt/CZ44-LSA after reduction at 453 K (filled bar) and (B) PtO_2 in Pt/CZ0-LSA calcined at 823 K (empty bar) and Pt in Pt/CZ0-LSA after reduction at 453 K (filled bar).

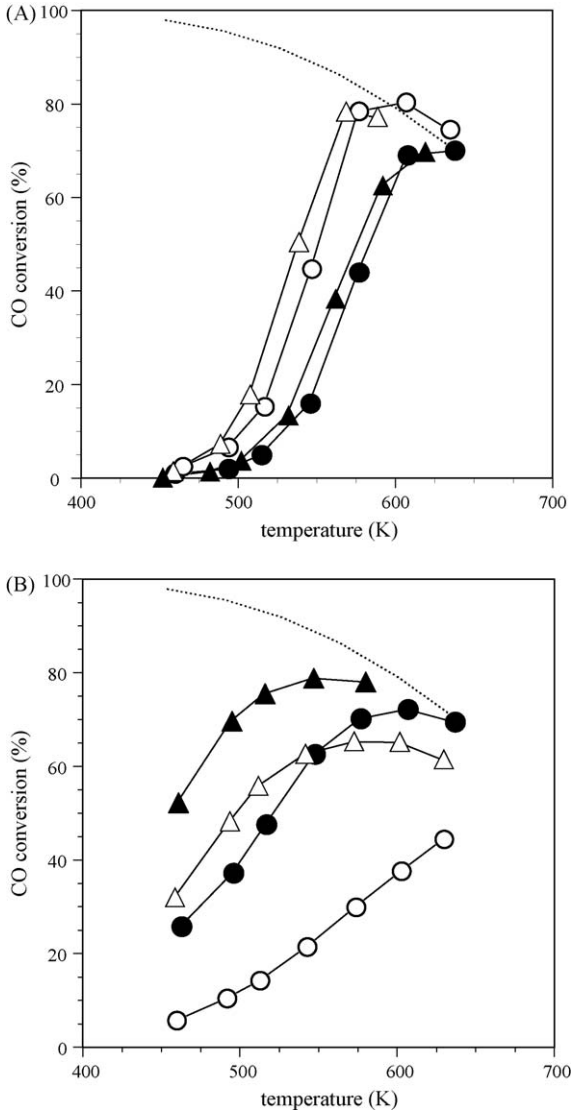

Fig. 5. CO conversion in WGS reaction after different calcination temperature. (A) Platinum catalyst supported on LSA CZ44 (●: 623 K and ○: 823 K) and on CZ0 (▲: 623 K and △: 823 K) and (B) gold on CZ44 (●: 523 K and ○: 723 K) and on CZ0 (▲: 523 K and △: 723 K). Operating conditions: 1 h pre-reduction under 5% H_2 (35 ml/min) at 453 K, GHSV = 40,000 h^{-1}; feeding composition 6% CO, 10% CO_2, 21% H_2O, 38% H_2, N_2 to balance.

Fig. 6 are related to platinum catalysts prepared from chloride precursors calcined at 623 K. The choice of such temperature of calcination meets the exigency of obtaining values of surface area comparable for both ceria–zirconia and zirconia catalysts and to limit possible effects of chlorides, which at this temperature are equally present in all supports (ca. 1 wt.%).

In the case of gold catalysts, HRTEM characterization (see Table 2) shows that the particle size distribution is quite narrow and comprised in the interval of 1.2–2.0 nm, with a maximum at 1.7 nm, in the Au/CZ44-HSA sample. This is only slightly lower compared to the value obtained for Au in the LSA samples (where distribution curve was centered at 2.0 nm) and suggests that the surface area of the support contributes only marginally to metal dispersion, which depends more on other parameters such as the concentration and pH of the $HAuCl_4$ solution used in the deposition procedure [34,36,45].

Platinum and gold catalysts behave differently also in relation to the composition of supports: gold shows a higher WGS activity if supported on pure zirconia while in the case of platinum the dependence on the support composition become relevant when platinum chlorides are used as precursors. Fig. 8 shows that platinum catalysts supported on zirconia and on ceria–zirconia have similar activity when prepared from nitrates, while a certain dependence on the type of support has been observed for the ex-chloride catalysts, with Pt(Cl)/CZ0-LSA performing better than Pt(Cl)/CZ44-LSA. In any case, the use of nitrate precursors leads to a shift of light-off curves to lower temperatures. This enhancement of catalytic activity using nitrates correlates very well with the improvement of platinum dispersion observed by HRTEM and chemisorption measurements.

The improvement of performance for ceria containing formulation in comparison with the zirconia supported catalyst when the catalysts have been prepared by platinum nitrate salt reveals also the importance of having an operating spillover mechanism in

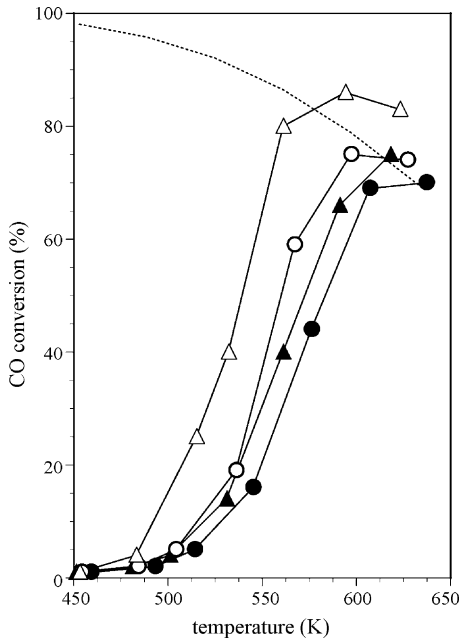

Fig. 6. CO conversion in WGS reaction of low surface (filled) and high surface area (empty) platinum catalysts supported on CZ44 (●, ○), CZ0 (▲, △) prepared from H_2PtCl_6 and calcined at 623 K. Operating conditions: 1 h pre-reduction under 5% H_2 (35 ml/min) at 453 K, GHSV = 40,000 h^{-1}; feeding composition 6% CO, 10% CO_2, 21% H_2O, 38% H_2, N_2 to balance.

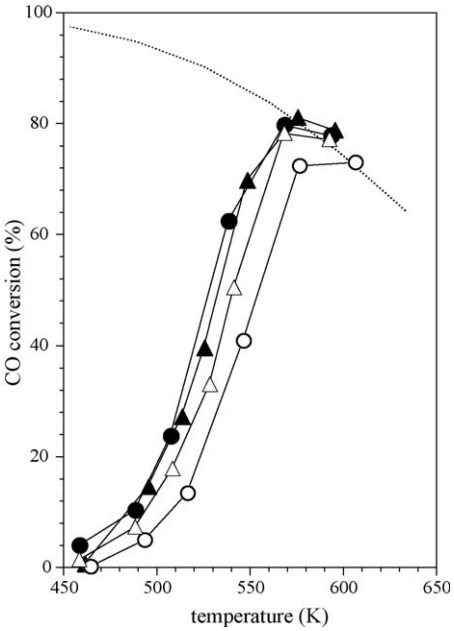

Fig. 8. CO conversion of LSA-platinum catalysts prepared from H_2PtCl_6 (empty) and $Pt(NH_3)_4(NO_3)_2$ (filled) and supported on CZ44 (●, ○), CZ0 (▲, △) calcined at 823 K. Operating conditions: 1 h pre-reduction under 5% H_2 (35 ml/min) at 453 K, GHSV = 40,000 h^{-1}; feeding composition 6% CO, 10% CO_2, 21% H_2O, 38% H_2, N_2 to balance.

order to obtain active low temperature WGS catalysts. In fact it is well known that the presence of chlorine at the metal-support interface of ceria-based catalysts can inhibit the spillover of adsorbed reactants from the metal to the support and vice versa [60,61]. Nevertheless, since the dependence of activity on the composition of support is almost negligible when the catalysts have been prepared from nitrate precursors, it is likely that oxygen storage capacity of the support, associated to the presence of ceria, plays only a secondary role on the WGS activity of the investigated compositions.

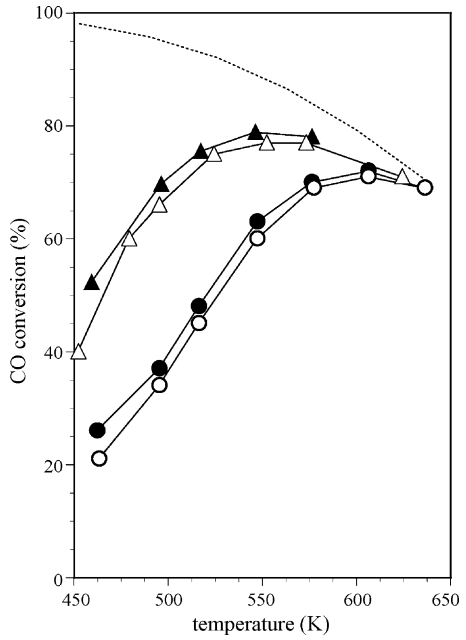

Fig. 7. CO conversion of low surface area (filled) and high surface area (empty) gold catalysts supported on CZ44 (●, ○), CZ0 (▲, △), prepared from $HAuCl_4$, and calcined at 523 K. Operating conditions: 1 h pre-reduction under 5% H_2 (35 ml/min) at 453 K, GHSV = 40,000 h^{-1}; feeding composition 6% CO, 10% CO_2, 21% H_2O, 38% H_2, N_2 to balance.

3.3. TPR measurements and discussion on the role of the properties of support

The interaction between metal and support and the redox properties of the studied compositions have been investigated by temperature programmed reduction using CO as reducing agent. In fact, in the TPR profiles, both the position and the area of the peaks at low temperature are related respectively to the nature of interaction between metal and support and to the reduction of the metal [46].

Figs. 9 and 10 show the CO-TPR profiles of platinum-supported catalysts. From the comparison of the results of ex-nitrate (bold lines) and ex-chloride catalysts (dotted lines), it is possible to see a correlation between the position of the low temperature reduction peak and the WGS activity of catalysts: the higher activities of ex-nitrate catalysts correspond to a shift at lower temperature of platinum reduction peak in comparison to what happens for ex-chloride catalysts. Fig. 10 shows more details on CO-TPR profiles of the ex-chloride platinum samples. The low temperature peak corresponds to more than 80% of reduction Pt and it is overlapped by the simultaneous reduction of the support. In this case the formation of CO_2 occurs together with a small production of H_2 (see Table 2 for quantitative results), which is due to the interaction between CO and OH groups present on the surface of the support oxide. This suggests that at low temperature, CO oxidation on platinum-based catalysts involves the removal of surface hydroxyl groups and also the extraction of oxygen ions from the bulk with formation of mobile vacancies. This is correlated with the shift activity of these samples. Recently on the basis of DRIFT and MS/SSITKKA studies on the Pt/ZrO_2 catalyst it has been proposed a simple redox mechanism involving activation of water at oxygen vacancies present on the surface of the zirconia adjacent to a Pt particle, followed by transfer of O_{ads} to the Pt particle, where it could react with CO to release CO_2 [62].

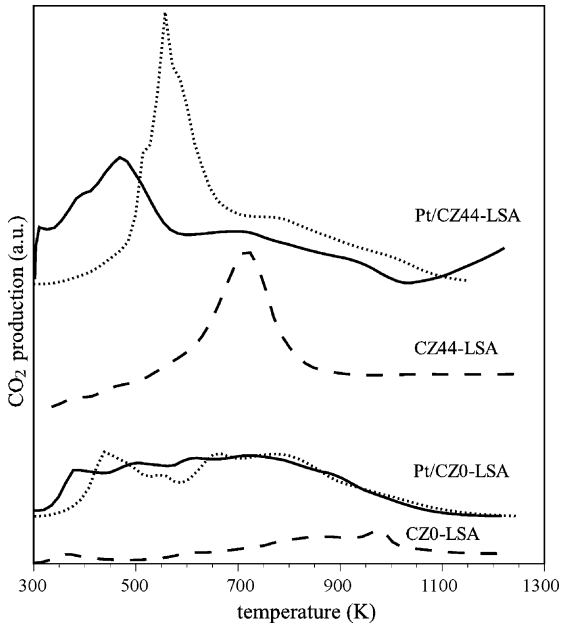

Fig. 9. CO-TPR profiles of supports (- - -) and of platinum catalysts prepared from chloride (· · ·) and nitrate (—) precursors.

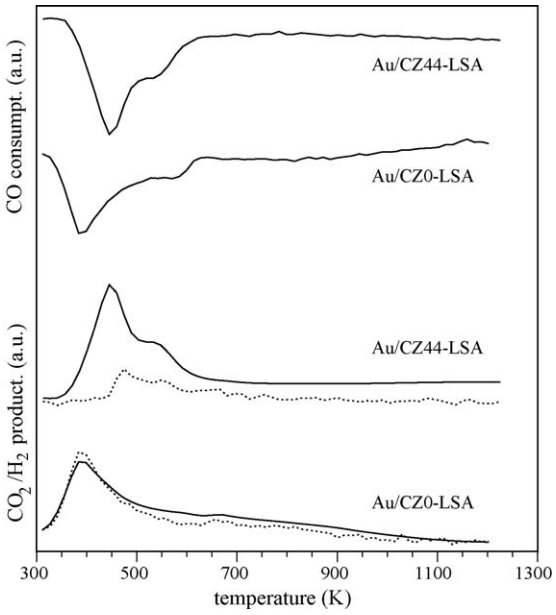

Fig. 11. CO-TPR profiles of gold catalysts: details of CO, CO_2 (—) and H_2 (· · ·) signals.

In literature a mechanism via formates [28,63] has been alternatively proposed. In this case the activity of platinum catalyst has been found dependent on the compositions of support and improved on ceria–zirconia mixed oxide in comparison to the pure oxides because of their higher reducibility [64]. Our results do not allow us to go further in the discussion concerning the mechanism of reaction, which would require the individuation of intermediates of reaction by appropriate in situ studies. However, from our findings it is possible to conclude that in platinum catalysts the active sites are most probably surface vacancies and interfacial defects, located mainly at the perimeter of metal particles.

On the contrary to what observed for platinum catalysts the activity of gold samples for the WGS reaction depends on the composition of support and it is substantially higher for gold supported on pure zirconia. Even in this case, TPR profiles of the catalysts are correlated with their WGS activities and can help to investigate the nature of interaction between gold and support. The maximum of CO_2 production of Au/CZ0-LSA occurs at lower temperature than that of Au/CZ44-LSA in agreement with the higher activity of the former (Fig. 11). Moreover, it is interesting to note that in the case of zirconia, the release of CO_2 occurs with a stoichiometric production of H_2. The results of the quantitative analysis are summarized in Table 3, where the last columns report the data relative to the integration of the peaks in the range of 300–500 K. Since the water gas shift mechanism involves the reaction of CO with water dissociatively adsorbed on the supports [65], the TPR results suggest the high WGS activity of zirconia relies on the possibility to easily form and remove hydroxyl groups on and from its surface. FTIR studies confirm that zirconia surface contains Brönsted acidic and basic hydroxyl groups and coordinatively unsaturated Lewis acidic-base Zr^{4+}–O^{2-} pairs that are stabilized by either a dissociative or non-dissociative adsorption of water molecules. It was also reported that on surface of highly hydrated zirconia, co-ordinated molecular water was eliminated upon evacuation at 450 K and various type of surface hydroxyls remain up to 873 K [37,66]. It is suggested that CO adsorbs preferably at a Zr-defective centre located at interface metal support, interacts with the adjacent O^{2-} and OH sites of zirconia forming bicarbonate, carbonate and/or formate species, that could be WGS intermediates. The presence of oxygen vacancies exposing coordinatively unsaturated Zr cations is consistent with the detection of Zr^{3+} centres on Au/ZrO_2 catalyst by EPR studies [67] and with a "junction" effect arising from the contact between the zirconia and nanosized gold particles [68].

In the case of the mixed oxide the production of CO_2 does not involve only the dehydroxylation of surface. In fact, production of CO_2 exceed those of hydrogen since the reduction is deeper and involves oxygen ions from the lattice. However Au/CZ44 is less active than Au/CZ0 and this excludes, as already observed for platinum catalysts, any relevance of redox properties of bulk in determining a high activity for water gas shift reaction. In this case, the lower activity of ceria–zirconia supported catalysts may be correlated with the structural change of zirconia induced by ceria doping. In fact ceria contributes to stabilize the cubic and

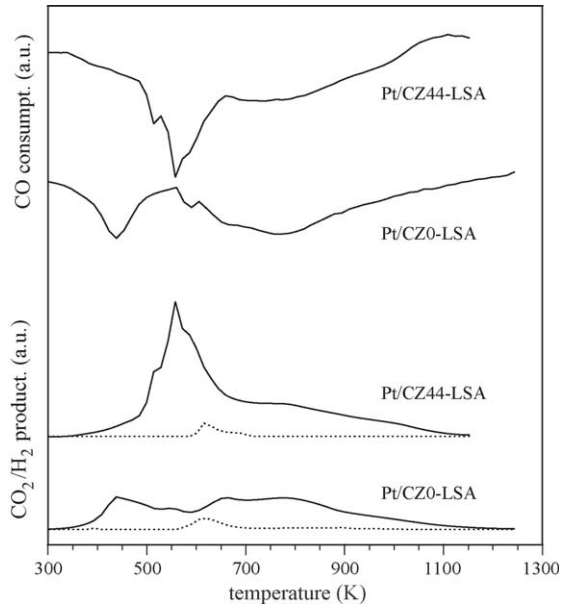

Fig. 10. CO-TPR profiles of platinum catalysts: details of CO, CO_2 (—) and H_2 (· · ·) signals of ex-chloride catalysts.

Table 3
TPR results.

Samples	Calcination temperature (K)	Total product./consumpt. (μmol/g)			First peak[a] product./consumpt. (μmol/g)		
		H_2	CO	CO_2	H_2	CO	CO_2
CZ44-LSA	1123	49	1581	1551			
CZ0-LSA	923	125	495	479			
Au/CZ44-LSA	523	346	1392	1412		943	943
Au/CZ0-LSA	523	747	1134	951	747	787	752
Pt(N)/CZ44-LSA	823	200	2161	2133		1147	1153
Pt(N)/CZ0-LSA	823	220	1212	1172	220	355	287
Pt(Cl)/CZ44-LSA	823	51	2050	1866		332	317
Pt(Cl)/CZ0-LSA	823	80	1420	1092		346	288

[a] Peak in the range of 300–500 K.

tetragonal polymorphisms of zirconia with respect to the monoclinic one. The former phases have been reported to be less active since they have a lower concentration of surface defects, which are able to promote the dissociative adsorption of water [38,69].

Taking into account that the nature of interface certainly plays a role in the decomposition of intermediates, the higher activity of zirconia-based catalyst could be also correlated to the nature of CO adsorption sites and to an electronic promotion of gold by zirconia. IR measurement [70] showed that the carbonyl band on metallic gold is shifted at much lower wavelength (2014 cm^{-1}) for Au/ZrO_2 in comparison to the values usually measured for ceria-based catalysts (around 2110–2090 cm^{-1}) [71]. The red shift of carbonyl band in the case of zirconia-based catalyst could be attributed to a negative charge on the metal clusters as suggested by Bocuzzi and coworkers for gold supported on titania [72] or to a strong interaction between CO and hydroxyl groups. The same type of interactions has been also reported for Au/ceria-based catalysts after reduction; for example the Au-carbonyl band at 2110 cm^{-1} shifts to 2097 cm^{-1} when $Au/Ce_{0.62}Zr_{0.38}O_2$ is reduced [71]. Bocuzzi and coworkers have also reported appearance of bands in the region 2090–2060 cm^{-1} in the spectra of reduced ceria or ceria–titania mixed oxides and have assigned them to CO adsorbed on negatively charged gold species [73,74]. A more detailed IR study goes beyond the scope of this work, however the result suggests that zirconia is able to alter the CO adsorption and desorption capacity of gold nanoparticles promoting the water gas shift reaction at lower temperature compared to ceria–zirconia.

4. Conclusions

In this work low temperature water gas shift activity of gold and platinum catalysts supported on zirconia and ceria–zirconia solid solution have been compared. It is pointed out that, at low temperature, gold catalysts have shown to be more active than those based on platinum. Moreover, we discussed the role of zirconia in promoting the activity of these systems, since this support has been found suitable in synthesizing gold and platinum active WGS catalysts. Doping zirconia with ceria allowed us to modify the redox and structural characteristics of support and to get insights into the parameters that affect the activity of these catalysts. The main conclusion is that, whatever the mechanism involved, the redox properties of support play a secondary role and more important is the nature of metal-support interface. It has been found that the synergism between precious metals and supports can be affected by the chosen parameters of synthesis and by the morphological and structural properties of support.

In the case of platinum catalysts the composition of support did not affect significantly the WGS activity that, conversely, was positively influenced by a very fine metal particles dispersion. Surface area and nature of precursors as well as new nanoparticle synthesis approaches are parameters to be optimized in order to improve the WGS activity of platinum catalysts. More important in promoting the activity of gold catalysts is the composition of support. Zirconia has been found to be a very suitable support for gold since it favors the dissociation of water and strongly interacts with gold particles to promote their capacity of adsorption and desorption of reactants involved on the reaction.

Acknowledgments

Authors thank Treibacher, Grace Davison Companies and MEL Chemicals to provide the supports and PRIN and MEC (ENE2006-06925) projects for the financial support.

References

[1] R. Farrauto, S. Hwang, L. Shore, W. Ruettinger, J. Lampert, T. Giroux, Y. Liu, O. Ilinich, Annu. Rev. Mater. Res. 33 (2003) 1.
[2] J.N. Armor, Catal. Lett. 101 (2005) 131.
[3] P. Giunta, N. Amadeo, M. Laborde, J. Power Sources 156 (2006) 489.
[4] J.M. Zalc, D.G. Löffler, J. Power Sources 111 (2002) 58.
[5] J.R. Ladebek, J.P. Wagner, in: W. Vielstich, H.A. Gasteiger, A. Lamm (Eds.), Handbook of Fuel Cells Fundamentals Technology and Applications, 2003, pp. 191–201.
[6] W. Ruettinger, O. Ilinich, R.J. Farrauto, J. Power Sources 118 (2003) 61.
[7] J. Pasel, P. Cremer, B. Wegner, R. Peters, D. Stolten, J. Power Sources 126 (2004) 112.
[8] C. Brooks, S. Cypes, R.K. Grasselli, A. Hagemeyer, Z. Hogan, A. Lesik, G. Streukens, A.F. Volpe, H.W. Turner, W.H. Weinberg, K. Yaccato, Top. Catal. 38 (2006) 195.
[9] A. Harayanto, S. Fernando, N. Murali, S. Adhikari, Energy Fuels 19 (2005) 2098.
[10] A.F. Ghenciu, Curr. Opin. Solid State Mater. Sci. 6 (2002) 389.
[11] R. Radhakrishnan, R.R. Willigan, T.H. Vanderspurt, Z. Dardas, AIChE J. 52 (2006) 1888.
[12] P. Panagiotopoulou, D.I. Kondarides, J. Catal. 225 (2004) 327.
[13] H. Iida, A. Igarashi, Appl. Catal. A 298 (2006) 152.
[14] A. Basinska, T.O. Maniecki, W.K. Jozwiak, React. Kinet. Catal. Lett. 89 (2006) 319.
[15] H. Iida, A. Igarashi, Appl. Catal. A 303 (2006) 192.
[16] R. Radhakrishnan, R.R. Willigan, Z. Dardas, T.H. Vanderspur, Appl. Catal. B 66 (2006) 23.
[17] E. Chenu, G. Jacobos, A.C. Crowford, R.A. Keogh, P.M. Patterson, D.E. Sparks, B.H. Davis, Appl. Catal. B 59 (2005) 45.
[18] S. Ricote, G. Jacobs, M. Milling, Y. Ji, P.M. Patterson, B.H. Davis, Appl. Catal. A 303 (2006) 35.
[19] D. Andreeva, Gold Bull. 35 (2002) 82.
[20] Q. Fu, A. Weber, M. Flytzani-Stephanopoulos, Catal. Lett. 77 (2001) 87.
[21] B.A.A. Silberova, G. Mul, M. Makkee, J.A. Moulijn, J. Catal. 243 (2006) 171.
[22] A. Venugopal, J. Aluha, M. Scurrel, Catal. Lett. 90 (2003) 1.
[23] V. Idakiev, T. Tabakova, Z.-Y. Yuan, B.-L. Su, Appl. Catal. A 270 (2004) 135.
[24] V. Idakiev, T. Tabakova, Z.-Y. Yuan, B.-L. Su, Appl. Catal. B 63 (2006) 178.
[25] T. Tabakova, V. Idakiev, K. Tenchev, F. Bocuzzi, M. Manzoli, A. Chiorino, Appl. Catal. B 63 (2006) 94.
[26] C.W. Corti, R.J. Holliday, D.T. Thompson, Appl. Catal. A 291 (2005) 253.
[27] D. Cameron, R. Holliday, D. Thompson, J. Power Sources 118 (2003) 298.
[28] G. Jacobs, S. Ricote, U.M. Graham, P.M. Patterson, B.H. Davis, Catal. Today 106 (2005) 259.
[29] Q. Fu, H. Saltsburg, M. Flytzani-Stephanopoulos, Science 301 (2003) 935.
[30] G. Jacobs, P.M. Patterson, L. Williams, E. Chenu, D. Sparks, G. Thomas, B.H. Davis, Appl. Catal. A 262 (2004) 177.
[31] A. Luengnaruemitchai, S. Osuwan, E. Gualari, Catal. Commun. 4 (2003) 215.
[32] F.C. Meunier, A. Goguet, C. Hardacre, R. Burch, D. Thompsett, J. Catal. 252 (2007) 18.
[33] C.D. Zeinalipour-Yazdi, A.L. Cooksy, A.M. Efstathiou, Surf. Sci. 602 (2008) 1858.
[34] T. Tabakova, F. Bocuzzi, M. Manzoli, J.W. Sobczak, V. Idakiev, D. Andreeva, Appl. Catal. A 298 (2006) 127.

[35] Q. Fu, S. Kudriavtseva, H. Saltsburg, M. Flytzani-Stephanopoulos, Chem. Eng. J. 93 (2003) 41.
[36] C. Zerva, C.J. Philippopoulos, Appl. Catal. B 67 (2006) 105.
[37] Z.-Y. Ma, C. Yang, W. Wei, W.-H. Li, Y.-H. Sun, J. Mol. Catal. A: Chem. 227 (2005) 119.
[38] J. Li, J. Chen, W. Sang, J. Liu, W. Shen, Appl. Catal. A 334 (2008) 321.
[39] B. Yoon, H. Hakkinen, M. Landman, A. Worz, A.S. Antonietti, J.M. Abbet, K. Juday, U. Heiz, Science 307 (2005) 403.
[40] T. Tabakova, V. Idakiev, D. Andreeva, I. Mitov, Appl. Catal. A 202 (2000) 91.
[41] A.A. Fonseca, J.M. Fisher, D. Ozkaya, M.D. Shannon, D. Thompsett, Top. Catal. 44 (2007) 223.
[42] R. Burch, Phys. Chem. Chem. Phys. 8 (2006) 5483.
[43] J. Kaspar, P. Fornasiero, in: A. Trovarelli (Ed.), Catalysis by Ceria and Related Materials, Imperials College Press, London, 2002.
[44] E. Aneggi, M. Boaro, C. de Leitenburg, G. Dolcetti, A. Trovarelli, J. Alloys Compd. 408–412 (2006) 1096.
[45] A. Wolf, F. Schüth, Appl. Catal. A 226 (2002) 1.
[46] M. Boaro, M. Vicario, C. de Leitenburg, G. Dolcetti, A. Trovarelli, Catal. Today 77 (2003) 407.
[47] D. Radivojevic, K. Seshan, L. Lefferts, Appl. Catal. A 301 (2006) 51.
[48] M. Comotti, W.C. Li, B. Spliethoft, F. Schüth, J. Am. Chem. Soc. 128 (2006) 217.
[49] N. Lopez, J.K. Nørskov, T.V.W. Janssens, A. Carlsson, A. Puig-Molina, B.S. Clausen, J.-D. Grunwaldt, J. Catal. 225 (2004) 86.
[50] M. Valden, S. Pak, X. Lai, D.W. Goodman, Catal. Lett. 56 (1998) 7.
[51] D. Tibiletti, A.A. Fonseca, R. Burch, Y. Chen, J.M. Fisher, A. Gouget, C. Hardacre, P. Hu, R.W. Hu, D. Thomsett, J. Phys. Chem. B 109 (2005) 22553.
[52] X. Wang, J.A. Rodriguez, J.C. Hanson, M. Pérez, J. Evans, J. Chem. Phys. 123 (2005) 221101.
[53] A. Goguet, R. Burch, Y. Chen, C. Hardacre, P. Hu, R.W. Joyner, F.C. Meunier, B.S. Mun, D. Thompsett, D. Tibiletti, J. Phys. Chem. C 111 (2007) 16927.
[54] Z.-P. Liu, S.J. Jenkins, D.A. King, Phys. Rev. Lett. 94 (2005) 196102.
[55] X. Zhang, H. Wang, Bo-Q. Xu, J. Phys. Chem. B 109 (2005) 9678.
[56] D. Duprez, Catal. Today 112 (2006) 17.
[57] Y. Denkwitz, A. Karpenko, V. Plzak, R. Leppelt, B. Schumacher, R.J. Behm, J. Catal. 246 (2007) 74.
[58] H. Sakurai, T. Akita, S. Tsubota, M. Kiuchi, M. Haruta, Appl. Catal. A 291 (2005) 179.
[59] C. Rhodes, G.J. Hutching, A.M. Ward, Catal. Today 23 (1995) 43.
[60] D.I. Kondarides, X.E. Verykios, J. Catal. 174 (1998) 52.
[61] A. Wootsch, C. Descorme, D. Duprez, J. Catal. 225 (2004) 259.
[62] D. Tibiletti, F.C. Meunier, A. Goguet, D. Reid, R. Burch, M. Boaro, M. Vicario, A. Trovarelli, J. Catal. 244 (2006) 183.
[63] G. Jacobos, S. Ricote, B.H. Davis, Appl. Catal. A 302 (2006) 14.
[64] P.S. Querino, J.R.C. Bispo, M.d.C. Rangel, Catal. Today 107–108 (2005) 920.
[65] D.C. Grenoble, M.M. Estadt, J. Catal. 67 (1981) 90.
[66] G. Cerrato, S. Bordiga, S. Barbera, C. Monterra, Appl. Surf. Sci. 115 (1997) 53.
[67] P. Claus, A. Brückner, C. Mohr, H. Hofmeister, J. Am. Chem. Soc. 122 (2000) 11430.
[68] J.S. Frost, Nature 334 (1988) 577.
[69] K.-H. Jacob, E. Knozinger, S. Benier, J. Mater. Chem. 3 (1993) 651.
[70] G. Busca, Spectra have been taken after exposing the reduced catalysts (1 hr under 5% H_2 in He 30 ml/min flow, at 453K) at 100 mbar of CO for 1 hr, private communication.
[71] S.E. Collins, J.M. Cies, E. del Rio, M. Lopez-Haro, S. Trasobares, J.J. Calvino, J.M. Pintado, S. Bernal, J. Phys. Chem. C 111 (2007) 14371.
[72] F. Boccuzzi, A. Chiorino, M. Manzoli, Surf. Sci. 454 (2000) 942.
[73] T. Tabakova, F. Bocuzzi, M. Manzoldi, D. Andreeva, Appl. Catal. A 252 (2003) 385.
[74] F. Vindigni, M. Manzoli, A. Chiodino, T. Tabakova, F. Boccuzzi, J. Phys. Chem. B 110 (2006) 23329.